PERFORMANCE OF PACKED-BED SYSTEMS AND COUPLING WITH BRAYTON CYCLES

David Pérez-Gallego[1,2,*], Julián Gonzalez-Ayala[1,2], Alejandro Medina[1,2], Antonio Calvo Hernández[1,2]

[1]Department of Applied Physics, Universidad de Salamanca, 37008 Salamanca, Spain

[2]Institute of Physics and Mathematics (IUFFYM), Universidad de Salamanca, 37008 Salamanca, Spain

*Corresponding Author: dpgallego@usal.es

ABSTRACT

Due to the increase in energy production through renewable sources, which are highly variable, it is necessary to stabilize their incorporation into the supply network and adjust it to the demand of the electrical network, which is highly variable as well. Energy storage is one of the most reliable solutions. It consists in storing energy during the hours of highest production, store it for the required period and supply at times of lower production or higher energy demand on the network. Therefore, systems that can store large amounts of energy for the increasing production scale are required. Today, storage systems based on hydro-pumping are the mostly commissioned due to their high storage capacity. However, a promising technology for storing energy at high temperatures is the pumped thermal energy storage system (PTES). Within PTES, a packed-bed (PB) subsystem allows direct coupling with a Brayton discharge cycle to extract the stored energy, thus, making possible to operate at high temperatures. Brayton cycles are relevant because they can achieve high-energy production without geographical restrictions.

Packed-beds consist of a tank filled with two phases: a solid phase (generally rocks or sand), with high heat capacity and capable of rising to high temperatures; and a liquid or gas phase, a hot fluid (air or liquid) circulating through the tank. Thermal energy can be stored for hours.

Due to the non-stationary nature of these systems, the charging and discharging numerical model is necessary to analyze the complex dependence on temperature in the interval of interest where the packed bed operates. Thus, it is essential to use techniques to solve the differential equations describing the dynamics within the packed-bed, and its temporal evolution. A secondary step is the TES system and Brayton cycle coupling for energy production.

This article contains a study on a 1-dimensional numerical modeling of a packed-bed with all its parameters. Afterwards, a simple model of PB integration in Brayton charging and discharging cycles using a CSP plant as a renewable source is presented. Once the integration is done, a sensitivity study is carried out on a charge/discharge cycle with a storage time of 20 hours. Total energy storage efficiencies of 0.52 are reported and as well as Brayton cycle efficiencies about 0.24 in addition to a power output of 2.5MW. For successive cycles, under steady state operation, the efficiency is increased to 0.67 due to the reduction in energy input, but a degradation of the thermocline decreases power output, compared with a single storage cycle.

1   INTRODUCTION

Electricity produced by intermittent renewable energy sources is increasing at a high rate worldwide. The development of novel clean energy technologies is nowadays essential because of the necessity to limit harmful and greenhouse emissions, the depletion of fossil fuels, prices variability, and the increasing electric energy demand. Moreover, the expected efforts to electrify the transport sector require to accelerate the deployment of renewable technologies. Nevertheless, the irregular nature of solar and wind resources makes difficult the dispatchable on-demand production of clean energy. Thus, low-cost and efficient electrical energy storage is basic to balance the mismatch between energy supply and demand.

Thus, an open challenge of the energy transition for the next years is to develop technological routes to efficiently produce electric energy in a renewable and clean way ensuring production control and dispatchability. Apart from initiatives such as the enhancement of grid interconnections or over-sizing renewable capacity, this is associated with large-scale energy storage (Olympios *et al*., 2021)

There exist several storage technologies at MW scales that are at dissimilar readiness levels. A possible way to classify energy storage technologies, as proposed by (Rahman *et al.,* 2020) encompasses:

- Mechanical: including pumped hydro, flywheels, compressed air storage (CAES, A-CAES, etc.) (Bartela *et al*., 2022), and liquid air energy storage (LAES) (Vecchi *et al*., 2021).
- Electrochemical: including secondary (PbA, Na-S, Li-ion, Ni-Cd, ...) and flow (vanadium redox and Zn-Br batteries).
- Chemical: hydrogen and synthetic fuels (Schäppi *et al*., 2021)
- Electrical: supercapacitors.
- Thermal Energy Storage (TES): sensible, latent heat, and thermo-chemical (Carrillo *et al*., 2019). Some technologies within CAES also can be considered as belonging to this category, as it will be commented on later, because have both mechanical and thermal elements. Pumped thermal energy storage (PTES) (Benato and Stoppato, 2018 and Pérez-Gallego *et al*. 2021) and Concentrating Solar Power (CSP) (Achkari and Fadar, 2020) can also be included here. Details on both will be exposed later in this Introduction.

This classification should not be considered rigid, but just as a simple reference guide, because some technologies involve different cross-concepts. Nowadays, pumped hydro energy storage by large constitutes the most deployed technology, constituting more than 90% of the total grid-scale storage (Steinmann *et al*., 2020), but it is constrained to regions with particular hydrological, meteorological, and seasonal conditions.

TES techniques have advantages that make them promising in the short- and mid-term. Two of them are remarkable: it benefits from relatively high energy densities (that should translate into a low cost per MWh of storage capacity) and its independence from geographical constraints (McTigue *et al*., 2015) (except for CAES). It is expected that in the next few years, TES can play a major role in large-scale renewable power production because of its direct integration in concentrated solar, wind, and photovoltaic technologies. Recent reviews on these concepts for different applications and their development stage are due to Olympios *et al*. (2021), McTigue *et al*. (2022) and Khan *et al*. (2022).

Concentrated solar power (CSP) technology is a promising in-development way to collect solar power and convert it into electricity through the heating of a heat transfer fluid. Among the reasons that make this renewable technology interesting for the near future two are remarkable: its high efficiency specially at high temperatures and the possibility to be combined with storage systems for supplying dispatchable electric energy to the grid, Merchán *et al*. (2022). In this work a central tower configuration will be selected. These configurations are the most deployed nowadays, mostly operating at intermediate temperatures through Rankine cycles and liquid thermal storage with molten salts. Nevertheless, there are intense efforts to couple the solar receiver to Brayton cycles operating at high temperatures using air as heat transfer fluid and solid thermal storage as, for instance, PB. The focus of this work is placed on the PB itself instead of the CSP subsystem. Models for central tower CSP systems were analyzed in previous works by our group (Merchán *et al*., 2020 and Merchán *et al*., 2022).

As stated before, PB thermal storage systems play a central role in technologies devoted to large-scale energy storage, in development nowadays. Apart from the peculiarities of each one, PB analysis has common ingredients, theoretical modeling schemes, and methodologies. Different kinds of researchers make use of PB possibilities and try to integrate them into particular frameworks (Petrollese *et al*., 2022). But theoretical modeling and the numerical methods required to obtain the aimed results are not trivial and there is a great dispersion in the literature.

This makes it difficult to select the theoretical model that better matches a particular problem and so, to develop a numerical scheme for the obtention of the particular intended results. Thus, the global aim of this paper is to develop a simple integration model between CSP, PB and open cycle Brayton cycle, using air as working fluid and with the real gas hypothesis. Among the results and conclusions, it is intended to show a PB assembly integrated into a CSP that supplies thermal energy for a certain time, evaluating the dimensions, power and charging/discharging times, in addition to the hysteresis cycles present in the PB with the continuous operation of its cycles.

2   PLANT SCHEME

The CSP has a central tower where the fluid is heated thanks to the heliostat field and a Brayton cycle for electric energy production. The coupling between packed-bed and Brayton cycle is shown in Fig. 1. There are three steps: charge, energy storage and discharge. Additionally, there is a packed bed incorporated to store thermal energy. It is used when solar irradiance decreases, as by night or for bad solar irradiance conditions. The Brayton cycle is an open cycle, it begins by taking the working fluid (air) from outside, it is filtered in the first filter, which is assumed adiabatic and has a small pressure drop, Δp=2%, this is stage (1)-(2). Then the air is compressed in a compressor in step (2)-(3). After compression, the fluid will go to the central solar receiver if it corresponds to the charging cycle or it will go directly to the PB if it corresponds to the discharge cycle, steps (3C)-(4C) and (3D)-(4D) respectively. In the charging cycle, after heating the working fluid in the central tower, a fraction of the flow will produce electricity in the turbine and a smaller part will store thermal energy in the PB, steps (4D)-(5) and (4C)-(packed-bed) respectively. In the discharge cycle, the fluid goes through the PB, where its temperature increases, step (3D)-(4D) and enters the turbine generating useful work, step (4D)-(5). Finally, the fluid is released to the outside through the last filter in step (5)-(6). As it is an open cycle, a low temperature PB is not required to cool the working fluid at the turbine outlet. To model the compressor and the expander, the isentropic efficiencies of both components will be assumed constant, see Table 1.
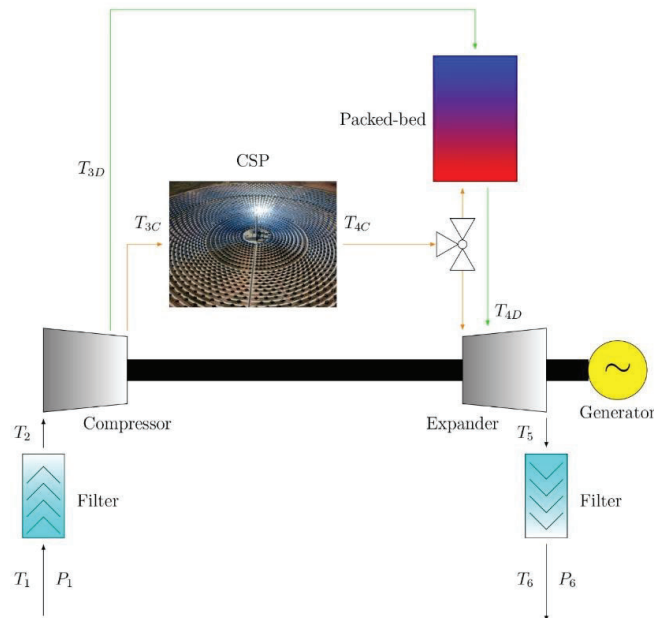
Figure 1: Plant scheme with Brayton cycle and packed-bed

3   BRAYTON SYSTEM

In the Brayton cycle model real properties of the working fluid were used, enthalpies, entropies, pressures, and temperatures are obtained from reported values at NIST provided through software Mathematica® ThermodynamicaData function.
The filters are assumed adiabatic, so:

$$h_2 = h_1; h_5 = h_6, \tag{1}$$

The isentropic efficiencies of compressor and turbine are assumed constant and independent of the compressor and expander mass flow:

37th INTERNATIONAL CONFERENCE ON EFFICIENCY, COST, OPTIMIZATION, SIMULATION AND ENVIRONMENTAL IMPACT OF ENERGY SYSTEMS, 30 JUNE - 4 JULY, 2024, RHODES, GREECE

3

$$\eta_c = \frac{h_3 - h_2}{h_{3s} - h_2}. \tag{2}$$

$$\eta_t = \frac{h_5 - h_4}{h_{5s} - h_4}. \tag{3}$$

The work per unit of time of the compressor and turbine is:

$$\dot{W}_c = \dot{m}(h_3 - h_2), \tag{4}$$

$$\dot{W}_t = \dot{m}(h_5 - h_4). \tag{5}$$

The heliostat field is not modelled in this paper. A constant temperature outlet from heliostat field is assumed (Merchán *et al.*, 2020).

The main data on the Brayton cycle of charging and discharging are summarized in Table 1. The pressure ratio in the compressor is r_p. Note that pressure ratio along charge is very small, this allows to use an electrical fan instead of a compressor for the fluid entering the packed-bed. However, the mass flow that enters the turbine after the solar receiver should be compressed at higher pressures, this technical problem is outside the scope of this study.

Table 1: Main parameters of Brayton cycle

	r_p	η_c	η_t
Charge	1.3	0.85	--
Discharge	5	0.85	0.9

4   PACKED-BED

Packed-bed system is used to store thermal energy. This system is made of a cylindrical tank of length L and diameter D. The heat transfer fluid (HTF) which runs through the interior is air with a thermal conductivity K_f, a heat capacity $c_{p,f}$ and a density ρ_f. It is filled with a storage material, in this case sand with a porosity of ε. Porosity is defined as the free space between particles, that is, the ratio between the empty volume within the bed and its total volume.

$$\varepsilon = 1 - \frac{V_{solid}}{V_{total}}. \tag{6}$$

The storage particles are modelled as spherical and have a diameter d_p.

Other important parameters are a_s defined as the ratio between the surface of the solid and the total volume and a_b defined as the ratio between the internal surface of the bed and the total volume.

$$a_s = \frac{6(1-\varepsilon)}{d_p}, \tag{7}$$

$$a_b = \frac{4}{D_{in}}. \tag{8}$$

Assuming a constant mass flow, $\dot{m}$, in the tank, the interstitial velocity of the fluid in the bed is:

$$u = \frac{\dot{m}}{\varepsilon \rho_f A_t}, \tag{9}$$

where $A_t = \pi(D_{int}/2)^2$.

The convective coefficient regulates the heat exchange between the fluid and the storage material (Esence *et al.*, 2017), this coefficient is given by:

$$h = \frac{K_f \cdot N_u}{d_p}, \tag{10}$$

where N_u is the Nusselt number defined as follows in terms of Prandtl and Reynolds numbers:

$$P_r = \frac{\mu_f \cdot c_{p,f}}{K_f}, \tag{11}$$

$$R_e = \frac{\varepsilon \cdot u \cdot d_p \cdot \rho_f}{\mu_f}, \tag{12}$$

$$N_u = 2.0 + 1.1 R_e^{0.6} \cdot Pr^{1/3}. \tag{13}$$

The general loss parameter establishes the total losses due to heat leaks through conduction, convection and radiation. More details about general loss parameter are given in Xie *et al.* (2022).

$$U^{-1} = r_{in} \cdot \left(\frac{1}{r_{in} \cdot h_{in}} + \sum_{n=1}^{N} \frac{ln(r_n/r_{n-1})}{K_n} + \frac{1}{r_{ext}(h_{ext}+h_{rad})} \right). \tag{14}$$

The parameters used to model the PB are detailed in Table 2.

Table 2: Packed-bed parameters.

Dimensions		
L [m]	D_{int} [m]	ε
6	3	0.39
HTF: air		
$\dot{m}$ [kg/s]	P [atm] Charge/Discharge	T_{max} [K]	T_{min}[K]
6.4	1.3/5	1200	298
Storage material: sand		
d_p [mm]	ρ_s [kg/m^3]	$c_{p,s}$ [J/(kg K)]	K_s [W/(mK)]
8	3550	902	0.5
Walls: carbon steel		
e_w [mm]	ρ_w[kg/m^3]	$c_{p,w}$ [J/(kg K)]	K_w [W/(mK)]
20	7900	477	51
Insulation: mineral wool		
e_{ins} [mm]	ρ_{ins}[kg/m^3]	$c_{p,ins}$ [J/(kg K)]	K_{ins} [W/(mK)]
200	32	835	0.038

Various models describe the heat transfer behavior of a PB. In this case, the continuous solid phase model will be used. It states a system of differential equations for the temperatures of the solid and the fluid arising from energy and mass conservation in the cylindrical tank (Ismail and Stuginsky, 1999):

$$\varepsilon \rho_f c_{p,f} \left(\frac{\partial T_f}{\partial t} + u \frac{\partial T_f}{\partial z} \right) = \frac{\partial}{\partial z} \left(K_f \frac{\partial T_f}{\partial z} \right) + h a_s (T_s - T_f) + U a_b (T_\infty - T_f), \tag{15}$$

$$(1-\varepsilon) \rho_s c_{p,s} \left(\frac{\partial T_s}{\partial t} \right) = \frac{\partial}{\partial z} \left(K_s \frac{\partial T_s}{\partial z} \right) + h a_s (T_f - T_s), \tag{16}$$

where T_f, T_s and T_∞ are the fluid, solid and ambient temperature respectively. These equations most be solved numerically, using the implicit Euler method. This method, within the finite-difference scheme, the derivatives are approximated by a spatial or temporal jump of the function:

$$T = T_n^t, \tag{17}$$

$$\frac{\partial T}{\partial t} = \frac{T_n^t - T_n^{t-1}}{\Delta t}, \tag{18}$$

$$\frac{\partial T}{\partial z} = \frac{T_n^t - T_{n-1}^t}{\Delta z}; \qquad \frac{\partial^2 T}{\partial z^2} = \frac{T_{n+1}^{t-1} - 2T_n^{t-1} + T_{n-1}^{t-1}}{\Delta z^2}. \tag{19}$$

Equations (9)-(16) will be solved for each Δz in each Δt. The pressure drops in packed-bed are less than 0.2% for the case of study, so they are negligible.

37th INTERNATIONAL CONFERENCE ON EFFICIENCY, COST, OPTIMIZATION, SIMULATION AND ENVIRONMENTAL IMPACT OF ENERGY SYSTEMS, 30 JUNE - 4 JULY, 2024, RHODES, GREECE

5

https://doi.org/10.52202/077185-0001

This model and our numerical implementation have been widely validated with numerous experimental data, for instance it is shown in Fig. 2 the comparison of our simulations and the experimental results by Cascetta *et al.* (2016).
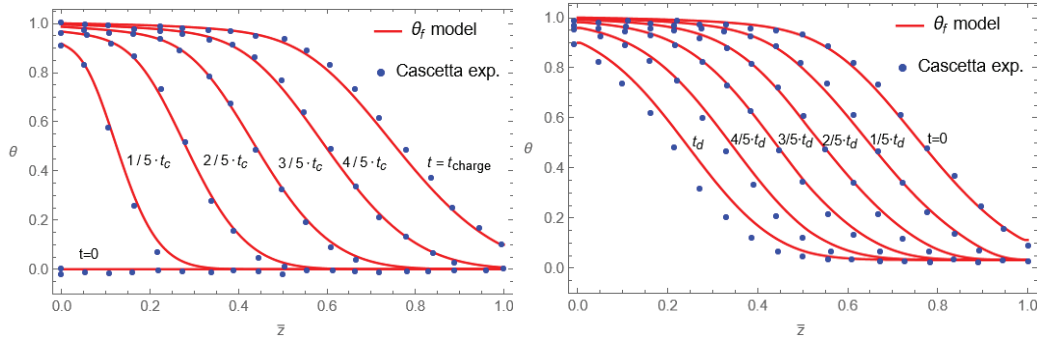
Figure 2: Model validation in charge (a) and discharge (b), comparing against the experimental results by Cascetta *et al.* (2016)

5   PERFORMANCE AND RESULTS

5.1   Charge

In the charge, the thermal energy of the CSP is used to produce electrical energy through the turbine and the generator. A surplus of this energy will be used in the thermal storage of the packed-bed, to be used later, when solar irradiance is zero. The charge of PB will conclude when the temperature of the fluid at the outlet of the bed reaches the following value: $(T_{max}+T_{min})/2$, where T_{max} is the maximum temperature reached in the PB and T_{min} is the minimum temperature measured in it. The stored energy and the inlet energy during charging are defined as follows:
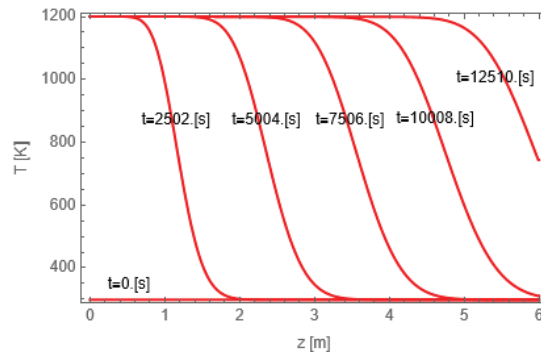
$$Q_{stored,c} = \int_0^L A_t \int_{T(t=0)}^{T(t=t_{charge})} [(1-\varepsilon)\rho_s c_{ps} + \varepsilon \rho_f c_{pf}] dT dz, \qquad (20)$$

$$Q_{input,c} = \int_0^{t_{charge}} \int_{T_f(t=0)}^{T_f(t=t_{charge})} \varepsilon A_t \rho_f c_{pf} u dT dt. \qquad (21)$$

Finally, the charging efficiency is:

$$\eta_c = \frac{Q_{stored,c}}{Q_{input,c}}. \qquad (22)$$

Figure 3 shows the bed charging temperature profile as function of position. As time passes, the thermal energy stored increases. Charging ends when the bed temperature at z=L reaches the set value $(T_{max}+T_{min})/2$.

Figure 3: Temperature profile of PB in charge

6

5.2   Thermal energy storage

To model the transient time between a charge and a discharge of the PB, the heat leaks which occur through cylinder walls by means of radiation, conduction and convection are considered. Likewise, it is assumed that the HTF pressure at which storage occurs is the ambient pressure. The time between a charge and a discharge can be hours or days, depending on weather conditions and power demand. Heat loss due to leakage during storage and storage efficiency is defined as follows:

$$Q_{stored} = \int_0^L A_t \int_{T(t=0)}^{T(t=t_{end})} [(1-\varepsilon)\rho_s c_{ps} + \varepsilon \rho_f c_{pf}] dT dz, \tag{23}$$

$$\eta_s = \frac{Q_{stored}(t=t_{end})}{Q_{stored,c}}, \tag{24}$$

where t_{end} is the total time of thermal energy storage between charge and discharge.

Figure 4 shows the bed temperature profile just after charging (red) and just after finishing the 20 hours of energy storage (blue). Over the course of this time, it can be seen how energy is lost through the walls of the PB, slightly decreasing the stored energy, but the storage efficiency remains high, as shown in Section 5.4. It is also observed how the thermocline begins to degrade due to heat conduction in the axial direction of the PB.
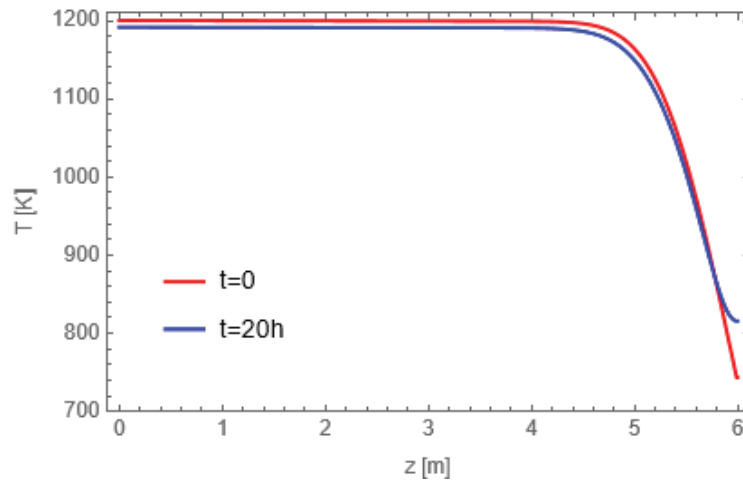
Figure 4: Temperature profile of PB in thermal energy storage. Time of energy storage from 0 to 20h

5.3   Discharge

During discharge, the energy previously stored in the packed-bed in the form of thermal energy is used to produce electrical energy using the expander and generator. During this phase the solar irradiance is zero, therefore it is a way to obtain energy when it would not otherwise be possible due to weather conditions.

The discharge begins by circulating the fluid at a low temperature in the opposite direction to that during charging, in this way it heats up and reaches a high turbine inlet temperature (TIT). The TIT should be approximately constant for a good performance of the turbine itself, therefore the discharge ends when the TIT begins to decrease. We define the energy recovered from the bed as well as the discharge efficiency as follows:

$$Q_{recovery} = \int_0^{t_{discharge}} \int_{T_{in}}^{T_{out}} \varepsilon A_t \rho_f c_{pf} u dT dt, \tag{25}$$

$$\eta_d = \frac{Q_{recovery}}{Q_{stored}(t=t_{end})}. \tag{26}$$

Figure 5 shows the temperature profiles at the bed discharge. The discharge begins in the opposite direction to the charge, that is, in this case the fluid enters from the right (in the plot) at z=L and flows

37ᵗʰ INTERNATIONAL CONFERENCE ON EFFICIENCY, COST, OPTIMIZATION, SIMULATION AND ENVIRONMENTAL IMPACT OF ENERGY SYSTEMS, 30 JUNE - 4 JULY, 2024, RHODES, GREECE

7

to the left (in the plot), until z=0. The discharge ends when the outlet temperature of the fluid at z=0 is no longer constant. It should be noted how the temperature of the fluid entering the bed is higher than the ambient temperature due to the heating suffered in the compression during the previous stage.
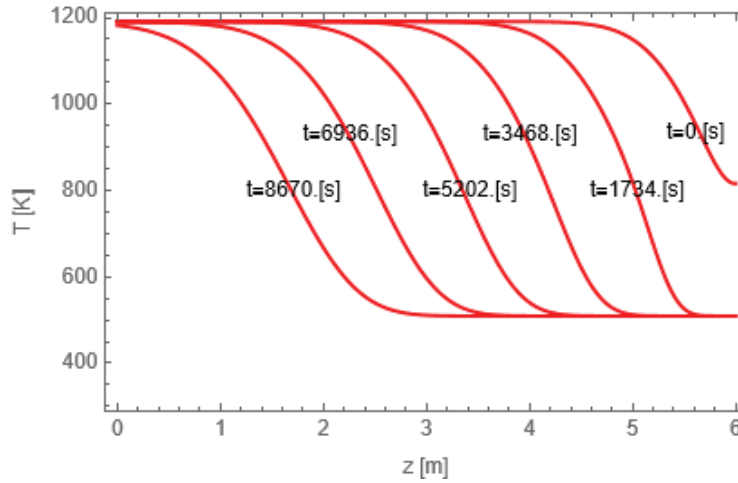

Figure 5: Temperature profile of PB in discharge

5.4 Overall system

The overall performance of the PB system is defined as:

$$\eta_t = \frac{Q_{recovery}}{Q_{input}} = \eta_c \eta_s \eta_d. \tag{27}$$

On the other hand, the total efficiency of the Brayton cycle is defined as η_b:

$$\eta_b = \frac{|W_t| - |W_c^{discharge}|}{|Q_{recovery}|} = \frac{|h_5 - h_{4D}| - |h_{3D} - h_2|}{|h_{4D} - h_{3D}|}. \tag{28}$$

Table 3: Heats and efficiencies for the packed-bed in the first cycle. Mass flux ratio is 6.4 kg/s.

Charge				
Q_{stored} [kWh]	Q_{input} [kWh]	Q_{output} [kWh]	η_c	t_{charge} [s]
20964	21799	831	0.968	12510
Energy storage between charge and discharge				
Q_{loss} [kWh]			η_s	t_{store} [s]
197			0.99	72000
Discharge				
$Q_{recovery}$ [kWh]	Q_{stored} [kWh]		η_d	$t_{discharge}$ [s]
11403	9341		0.55	8670
Round trip (overall cycle)				
η_t	$Q_{total,loss}$ [kWh]			
0.52	1056			
Brayton cycle in discharge				
W_c^{charge} [kWh]	$W_c^{discharge}$ [kWh]	W_t [kWh]	P_{out} [kW]	η_b Ideal (r_p=5)	η_b Real
440	3305	6065	2518	0.369	0.242

The Brayton cycle is only studied during discharge, with a pressure ratio of 5 and negligible pressure drops in the packed-bed. In the charge it would be possible to circulate a fraction of the mass flow heated up in the receiver through the cylindrical tank using some compression device, not explicitly considered in this paper. In addition, it is assumed that turbomachinery only works at design conditions, so the discharge stops when the TIT starts to decrease.

Table 3 shows the numerical values of the results obtained for one charge and discharge cycle. There are low pressure drops due to the low HTF velocity inside PB.
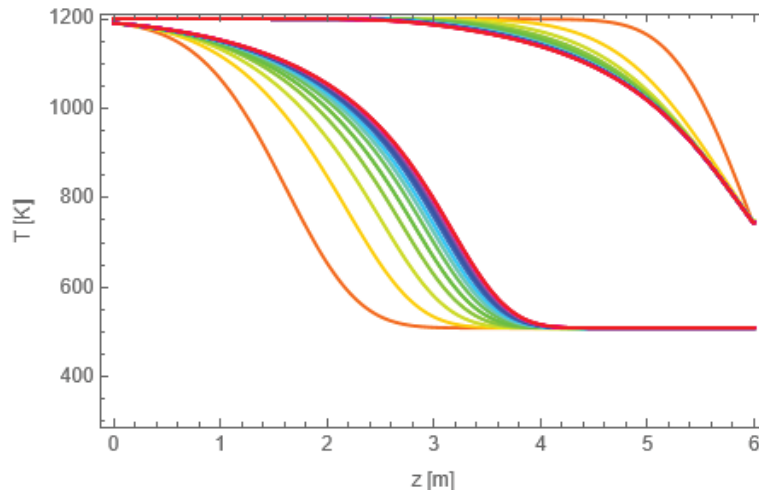
6   HYSTERESIS LOOPS

A study of the efficiency of each cycle is carried out. A single cycle consists of a charge followed by a discharge, in this case without an intermediate storage time. A total of 15 consecutive charge/discharge cycles are carried out. In Table 4 it is observed how the efficiency increases from the first cycle, this is due to the fact that the $Q_{recovery}/Q_{input}$ ratio increases since the energy stored in the previous cycle makes a smaller amount of Q_{input} necessary for reaching the final charging condition of subsequent cycles. Likewise, the $Q_{total,loss}$ increases due to the degradation of the thermocline, fundamentally this is lost in the charge due to the hot fluid which leaves the bed. With each successive cycle the total discharge time decreases due to the degradation of the thermocline, which results in less useful energy being obtained in the expander, however the power and total performance of the Brayton cycle remain constant. It seems contradictory that efficiency increases as the thermocline degrades with successive cycles from the initial one. However, as it has been mentioned, it is because at the steady state (from cycle 3 or 4) the energy introduced during charge is lower than the initial one. Therefore, $Q_{recovery}$ and Q_{input} are reduced in such a way that the total efficiency increases.

Figure 6 shows how it moves towards a steady state with each cycle, creating a figure of hysteresis cycles. The successive cycles are plotted towards the center of the panel, where the thermocline decreases.

Table 4: Heats and efficiencies for some cycles. P_{out} is 2.52 MW and η_b is 0.242.

Cycle	η_t	$Q_{total,loss}$ [kWh]	W_t [kWh]
1	0.52	1056	6065
2	0.64	3990	5120
3	0.66	3803	4616
4	0.66	3522	4260
5	0.67	3315	3987
10	0.67	2692	3148
11	0.67	2601	3022
12	0.67	2544	2917
13	0.67	2454	2812
14	0.67	2384	2707
15	0.67	2316	2623

37th INTERNATIONAL CONFERENCE ON EFFICIENCY, COST, OPTIMIZATION, SIMULATION AND ENVIRONMENTAL IMPACT OF ENERGY SYSTEMS, 30 JUNE - 4 JULY, 2024, RHODES, GREECE

9

Figure 6: Hysteresis loops of packed-bed. Discharge just after charge. Cycle 1 plotted in outer curves and Cycle 15 plotted in inner curves

7   CONCLUSIONS

A coupling of a simple Brayton cycle model and a more elaborated sand-air PB model has been developed. The isentropic efficiencies of the compressor and expander have been considered constant and independent of the mass flow. The PB model is a continuous solid phase model solved using the implicit Euler algorithm. The modelled system is subjected to a charge of 3.5 hours and afterwards 20 hours of storage, the bed is discharged. The discharge ends when the outlet temperature of the PB fluid is no longer constant and begins to decrease since the expander should operate at a constant temperature to guarantee on-design performance. For the first cycle, a storage efficiency of 0.52 and a Brayton cycle efficiency of 0.242 are obtained. For successive cycles, the storage performance improves, since it is half-charged from the previous cycles, the discharge power as well as the efficiency of the Brayton cycles remains constant. The problem arises from the degradation of the thermocline in each cycle, which prevents extracting the same amount of energy as the previous cycle, therefore although efficiency improves, the total energy recovered decreases. Solutions to avoid the degradation of the thermocline must be investigated, such as the variation of the mass flow in the cycles following the first.

NOMENCLATURE

a_b	Ratio between internal surface and volume of packed-bed	(m^{-1})
a_s	Ratio between storage material surface and packed-bed volume	(m^{-1})
Bi	Biot number	
c_p	Specific heat capacity	$(J/(kg\ K))$
d_p	Diameter of bed particles	(m)
D	Diameter of bed	(m)
h	Convection coefficient	$(W/(m^2\ K))$
K	Thermal conductivity	$(W/(m\ K))$
L	Packed-bed length	(m)
$\dot{m}$	Mass flux	(kg/s)
Un	Nusselt number	
Pr	Prandtl number	
Q	Heat	(J)
R_e	Reynolds number	
u	Interstitial velocity	(m/s)

U	Effective heat loss coefficient	(W/(m² K))

U   Effective heat loss coefficient $(W/(m^2\ K))$
W   Work (J)

Greek letters
ε   Void fraction or porosity
η   Efficiency
μ   Dynamic viscosity $(Pa\ s)$
ρ   Mass density (kg/s)

Subscript
c   Compressor
f   Heat transfer fluid
∞   Ambient temperature
max   Maximum
min   Minimum
s   Storage material
t   Turbine

Acronyms
TES   Thermal Energy Storage
TIT   Turbine Inlet Temperature
CAES   Compressed Air Energy Storage
LAES   Liquid Air Energy Storage
CSP   Concentrated Solar Power
HTF   Heat Transfer Fluid
PB   Packed-bed
PTES   Pumped Thermal Energy Storage

REFERENCES

Achkari, O., El Fadar, A., 2020, Latest developments on TES and CSP technologies-Energy and environmental issues, applications and research trends, *Appl. Therm. Eng*. 167, 114806.

Bartela, L., Ochmann, J., Lutynski, M., Waniczek, S., Smolnik, G., Rulik, S., 2022, Evaluation of the energy potential of an adiabatic compressed air energy storage system based on a novel thermal energy storage system in a post mining shaft, *J. Ener. Storage* 54, 105282.

Benato, A., Stoppato, A., 2018, Pumped thermal electricity storage: A technology overview, *Thermal Science and Engineering Progress*, vol. 6, p. 301-315.

Carrillo, A. J., González-Aguilar, J., Romero, M., Coronado, J. M., 2019, Solar energy on demand: A review on high temperature thermochemical heat storage systems and materials, *Chem. Rev*. vol. 119, p. 4777-4816.

Cascetta, M., Cau, G., Puddu, P., Serra, F., 2016, A comparison between CFD simulation and experimental investigation of a packed-bed thermal energy storage system, *Applied Thermal Engineering*, vol. 98, p. 1263-1272.

Esence, T., Bruch, A., Molina, S., Stutz, B., Fourmigué, J.-F., 2017, A review on experience feedback and numerical modeling of packed-bed thermal energy storage systems, *Solar Energy*, vol. 153, p. 628–654.

Ismail, K. A., Stuginsky Jr, R., 1999, A parametric study on possible fixed bed models for PCM and sensible heat storage, *Applied Thermal Engineering*, vol. 19 (7), p. 757-788.

Khan, M. I., Asfand, F., Al-Ghamdi, S. G., 2022, Progress in research and technological advancements of thermal energy storage systems for concentrated solar power, *J. Ener. Sto*., 55, 105860.

McTigue, J. D., Farres-Antunez, P., Sundarnath, K., Markides, C. N., White, A. J., 2022, Techno-economic analysis of recuperated Joule-Brayton pumped thermalenergy storage, *Ener. Conv. Manage*.

37th INTERNATIONAL CONFERENCE ON EFFICIENCY, COST, OPTIMIZATION, SIMULATION AND ENVIRONMENTAL IMPACT OF ENERGY SYSTEMS, 30 JUNE - 4 JULY, 2024, RHODES, GREECE

11   https://doi.org/10.52202/077185-0001

McTigue, J. D., White, A. J., Markides, C. N., 2015, Parametric studies and optimisation of pumped thermal electricity storage, *Appl. Ener.*, vol. 137 800– 811.

Merchán, R. P., Santos, M. J., Heras, I., González-Ayala, J., Medina, A., Calvo Hernández A., 2020, On-design pre-optimization and off-design analysis of hybrid Brayton thermosolar tower power plants for different fluids and plant configurations, *Renew. Sust. Ener. Rev.*, vol 119, 109590.

Merchán, R. P., Santos, M. J., Medina, A., Calvo Hernández A., 2022, High temperature central tower plants for concentrated solar power: 2021 overview, *Renew. Sust. Ener. Rev.*, vol 155.

Olympios, A. V., McTigue, J. D., Farres-Antunez, P., Tafone, A., Romagnoli, A., Li, Y., Ding, Y., Steinmann, W. D., Wang, L., Chen, H., Markides, C. N., 2021, Progress and prospects of thermos-mechanical energy storage: a critical review, *Progress in Energy*, vol 3, 022001

Pérez-Gallego, D., Gonzalez-Ayala, J., Calvo Hernández, A., Medina, A., 2021, Thermodynamic performance of a Brayton pumped heat energy storage system: Influence of internal and external irreversibilities, *Entropy,* vol. 23 (12) 1564.

Petrollese, M., Cascetta, M., Tola, V., Cocco, D., Cau, G., 2022, Pumped thermal energy storage systems integrated with a concentrating solar power section: Conceptual design and performance evaluation, *Energy,* vol. 247

Rahman, M. M., Oni, A. O., Gemechu, E., Kumar, A., 2020, Assessment of energy storage technologies: A review, *Ener. Conv. Manage*. 223, 113295.

Schäppi, R., Rutz, D., Dähler, F., Muroyama, A., Haueter, P., Liliestam, J., Patt, A., Furler, P., Steinfeld, A., 2021, Drop-in fuels from sunlight and air, *Nature*, vol. 601, p. 63-80.

Steinmann, W. D., Jockenhöfer, H., Bauer, D., 2020, Thermodynamic analysis of high-temperature Carnot battery concepts, *Energy Technology*, vol. 8 1900895.

Vecchi, A., Li, Y., Ding, Y., Mancarella, P., Sciacovelli, A., 2021, Liquid air energy storage (LAES): A review on technology state-of-the-art, integration pathways and future perspectives, *Advances in Applied Energy*, vol. 3 100047.

Xie, B., Baudin, N., Soto, J., Fan, Y., Luo, L., 2022, Wall impact on efficiency of packed-bed thermocline thermal energy storage system, *Energy*, vol. 247, 123503.

37th INTERNATIONAL CONFERENCE ON EFFICIENCY, COST, OPTIMIZATION, SIMULATION AND ENVIRONMENTAL IMPACT OF ENERGY SYSTEMS, 30 JUNE - 4 JULY, 2024, RHODES, GREECE

https://doi.org/10.52202/077185-0001   12